HHS Public Access

Author manuscript

J Control Release. Author manuscript; available in PMC 2020 January 10.

Published in final edited form as:

J Control Release. 2019 January 10; 293: 84–93. doi:10.1016/j.jconrel.2018.11.015.

Drug-Free Albumin-Triggered Sensitization of Cancer Cells to Anticancer Drugs

Lian Li[1], **Jiyuan Yang**[1], **Sirima Soodvilai**[1,2], **Jiawei Wang**[1], **Praneet Opanasopit**[2], and **Jindřich Kopeček**[1,3,*]

[1]Department of Pharmaceutics and Pharmaceutical Chemistry/Center for Controlled Chemical Delivery, University of Utah, Salt Lake City, Utah 84112, USA [2]Faculty of Pharmacy, Silpakorn University,NakhonPathom, Thailand [3]Department of Bioengineering, University of Utah, Salt Lake City, Utah 84112, USA

Abstract

Chemosensitization strategies have been used to sensitize cancer cells to conventional drugs, but their utility is often obstructed by additional off-target toxicity, limited access to intracellular targets and heterogeneous tumor pathogenesis. To address these challenges, we rationally developed a drug-free human serum albumin (HSA)-based therapeutic (KH-1) that functions extracellularly and exhibits pleiotropic effect on multiple intracellular signaling pathways. It is a two-step touch-trigger system that consists of a pretargeting anchor on surface receptor CD20 (anti-CD20 Fab' conjugated with a morpholino oligonucleotide 1) and a CD20 clustering actuator (HSA grafted with multiple copies of complementary morpholinooligonucleotide 2). The extracellular actuation by surface CD20 crosslinking boosts robust activations of numerous intracellular responses, and promotes cancer cell susceptibility to various anticancer drugs, including docetaxel (microtubule stabilizer), gemcitabine (nucleoside analogue) and GDC-0980 (PI3K/mTOR inhibitor). The broad applicability of KH-1 is demonstrated to result from simultaneous inhibition of survival pathways and augmentation of apoptotic pathways. In addition, KH-1 covalently conjugated with anthracycline anticancer agent, epirubicin, integrates the advantages of both chemosensitization function and improved intracellular drug delivery in a single system and takes effect on the same cell. Therefore, in the present study, we have provided mechanistic demonstration that crosslinking of surface receptors can be leveraged to elicit chemosensitization.

[*]To whom correspondence should be addressed (J. Kopeček): University of Utah, Center for Controlled Chemical Delivery, 2030 East 20 South, Biopolymers Research Building, Room 205B, Salt Lake City, Utah 84112-9452, USA. *Tel.*: +1 (801) 581-7211; *Fax*: +1 (801) 581-7848, jindrich.kopecek@utah.edu.

Conflict of Interest

J.Y and J.K. are co-inventors on a pending US patent application (PCT/US2014/023784; assigned to the University of Utah) related to this work. Otherwise, the authors declare no competing financial interests.

Keywords

drug-free macromolecular therapeutics; receptor crosslinking; chemosensitization; human serum albumin; signal transduction

1. Introduction

Cancer chemosensitization strategies have been developed to promote the efficacy of conventional drugs [1-7]. However, their effectiveness is constantly hindered by various challenges. Because the threshold elevation of cell response to anticancer agents is multifactorial due to heterogeneous tumor pathogenesis [8-10], sensitizers specific to a particular pathway or oncogene are not always operative. Furthermore, sufficient delivery of small molecular drugs, inhibitors, modulators or siRNA to their subcellular sites of action is difficult, which requires overcoming multiple barriers including cell uptake, lysosome escape and even mitochondrial localization/nucleopore penetration [11-14]. Worse still, numerous chemical sensitizers exacerbate systemic toxicity with additional off-target side effects, such as doxorubicin-mediated cardiotoxicity [15, 16]. As such, all these obstacles underscore the need to circumvent them *via* a drug (toxin)-free sensitization strategy that functions extracellularly and has a pleiotropic effect on different signaling targets.

Transmembrane receptors provide an ideal link from the exterior of cells to intracellular signal propagation, as they process an extracellular domain for binding of ligands and an intracellular domain for interference with signaling proteins [17-19]. Ligation of death receptors drives a series of pathways leading to caspase-8 activation and initiates extrinsic apoptosis [20]. Similarly, multivalent binding of Frizzled7 receptors inhibits Wnt signaling, a hyperactive driving force behind tumor progression [21]. In addition, our group demonstrated cell surface amplification of CD20 crosslinking overcomes rituximab resistance through augmenting numerous downstream pathways (*e.g.* calcium influx, NF-κB, mitochondrial pathway) [22-24]. In this regard, one prerequisite for optimal signal transduction that they share in common is the efficient clustering of these receptors. For example, conatumumab and rituximab that target death receptor 5 and CD20, respectively, have no activity unless hyper-crosslinked [25, 26]. Building upon these previous studies, which suggested a cascade of intracellular signaling could be manipulated by extracellular receptor crosslinking, we explored to leverage this extracellular actuation as a drug-free means to modulate numerous pathways for cancer cell chemosensitization.

Herein, a two-step touch-trigger approach, consisting of a pretargeting anchor on surface CD20 (anti-CD20 Fab' conjugated with a morpholino oligonucleotide 1, Fab'-MORF1) and an albumin actuator for triggering CD20 clustering (human serum albumin (HSA) grafted with multiple copies of complementary morpholino oligonucleotide 2, HSA-$(MORF2)_x$), is applied to boost robust activation of multiple innate signaling, in order to reset cell susceptibility to chemotherapeutics. Fab'-MORF1 acts as a bispecific engager that simultaneously binds CD20 receptor (*via* CD20-Fab′ biorecognition) and HSA-$(MORF2)_x$ (*via* MORF1-MORF2 hybridization). HSA is selected for its superior biocompatibility, stability, blood retention property, and its capability to load a vast array of drugs and ligands

[27]. We also take advantage of one disadvantage that HSA exhibits poor penetration into cells for the extracellular actuation [28]. Thus, the multivalent binding of CD20-bound Fab'-MORF1 by HSA-$(MORF2)_x$ is expected to act as a surface switch that directly transduces extracellular receptor crosslinking input into intracellular signal activation output, thereby enhancing the apoptosis of drug-treated cancer cells. Ultimately, our result reveals this drug-free HSA-based therapeutics (KH-1) indeed sensitizes cells to drugs with distinct mechanisms of action *via* simultaneous inhibition of survival pathways and activation of apoptosis pathways.

2. Materials and methods

2.1 Synthesis and Characterization

Fab'-MORF1 and Fab'-MORF1-Cy5 were synthesized based on our previously published methods [22-24]. HSA-$(MORF2)_x$ and HSA-$(MORF2)_x$-Cy3 with different valences were prepared by maleimide functionalization of HSA surface followed by thiol-ene reaction. Briefly, HSA was dissolved in PBS (pH 7.4) and the surface amino groups were converted to maleimide group by reaction with succinimidyl-[(*N*-maleimidopropionamido)-diethyleneglycol] ester ($SM(PEG)_2$ dissolved in dimethyl sulfoxide) at room temperature for 2 h (molar ratio of [HSA]:[$SM(PEG)_2$]= 1:55). The excess $SM(PEG)_2$ was removed by ultrafiltration (30,000 cut-off) five times to yield HSA-mal. The maleimide content in HSA was 33 maleimide groups per HSA molecule as measured by modified Ellman's assay. MORF2 with a free thiol end group was generated as previously described [22]. The freshly prepared MORF2-SH was added into HSA-mal solution in PBS (pH 6.5) and kept stirring at room temperature for 3 h. To obtain the HSA-$(MORF2)_x$ with different valences, the feeding molar ratios of HSA-mal to MORF2-SH were 1:2, 1:10, 1:20, and 1:30. At the end, unreacted MORF2-SH was removed by ultrafitration (30,000 Da cut-off) with 4 times PBS (pH 7.4). The MORF content was determined by UV-visible spectrophotometry at 260 nm in 0.1 N HCl (252120 $M^{-1}cm^{-1}$) and HSA content was quantified by bicinchoninic acid (BCA) protein assay (Pierce). To prepare HSA-$(MORF2)_x$-Cy3, HSA was labeled with 2 equivalents of cyanine 3 monosuccinimidyl ester (Cy3-NHS, Lumiprobe, Hunt Valley, MD) by 2 h reaction with surface amino groups at room temperature. The excess Cy3-NHS was removed by PD-10 column and ultrafiltration (30,000 cut-off) 4 times with PBS (pH 7.4) to yield HSA-Cy3. The following maleimide modification and MORF2 conjugation procedures were the same as described above. Epirubicin (EPI)-loaded HSA conjugates were fabricated using previously described procedures [29, 30]. Briefly, epirubicin hydrochloride (1mg/mL) in PBS (pH8.0) was thiolated by reacting with1 equivalent 2-iminothiolane (Traut's reagent) at room temperature for 2 h. Then, HSA-mal described above and HSA-$(MORF2)_x$ (still containing 15 remaining maleimide groups per HSA molecule after MORF2 conjugation according to modified Ellman's assay) were reacted with thiolated EPI in PBS for 2 h at room temperature (molar ratio of [HSA]:[EPI]= 1:60). Unconjugated EPI was removed by PD-10 column and final products were further purified by ultrafiltration (30,000 cut-off) 4 times with PBS (pH 7.4) to yield HSA-EPI and HSA-$(MORF2)_x$-EPI. The EPI content was determined by UV-visible spectrophotometry at 490 nm in PBS (pH 7.4).

2.2 Cell Culture

Raji B-lymphoma cells were cultured in RPMI-1640 medium (Gibco) supplemented with 10% fetal bovine serum (FBS) and 1% penicillin–streptomycin. Cells were suspended and cultured in T25 cellculture flasks and incubated at 37 °C in a humidified 5% CO_2 atmosphere.

2.3 Confocal Imaging

Raji cells were first exposed to 1 μM Fab'-MORF1 or Fab'-MORF1-Cy5 for 1 h at 37 °C. Then, cells were washed with cold PBS twice to remove unbound Fab'-MORF1 or Fab'-MORF1-Cy5. Afterward, cells were treated with HSA-mal-Cy3 (1 μM HSA), HSA-$(MORF2)_{1.4}$-Cy3 (1 μM MORF2), or HSA-$(MORF2)_{11.4}$-Cy3 (1 μM MORF2) for 5 h 37 °C. Intracellular lysosomes were stained with the lysotracker green DND-26 (Thermo Scientific) for 30 min and the nuclei within the cells were stained with 5 μg/mL Hoechst 33392 (Thermo Scientific) for 5 min. After washed with cold PBS three times, Raji cells were suspended in PBS in 4 well chambers prior to confocal visualization.

2.4 Enzymatic removal of the surface-bound Fab'-MORF1

After Raji cells were given the consecutive treatments as described above, the surface CD20-bound Fab'-MORF1-Cy5 were enzymatically digested , according to a previously published protocol [22], to remove the extracellular binding nanoconjugates and analyze the intracellular internalization. Briefly, cells were washed with cold PBS after the treatments, and then incubated with 0.4 mg/mL proteinase K (Thermo Scientific) for 20 min at 37 °C to degrade surface CD20. Afterward, the degradation was stopped by neutralizing the proteinase K with the same volume of 10% FBS containing cell culture medium (FBS stops the enzymatic activity). Then the detached nanoconjugates were removed by washing the cells with cold PBS twice, prior to flow cytometry analysis for intracellular fluorescence of Cy5 and Cy3.

2.5 Calcium Influx Analysis

Time-dependent changes in intracellular Ca^{2+}after various treatments were determined by flow cytometry-based quantification of intracellular calcium indicator Fluo-3AM (Thermo Scientific) fluorescence intensity. Raji cells(4×10^5), pretreated with Fab'-MORF1 (1μM, 1 h) and loaded with Fluo-3AM (5 μM, 30 min), were excited at 488 nm and the emission at 530 nm was measured on flow cytometry. A baseline was obtained for 120 s before the stimulation with (i) HSA-mal, (iii) HSA-$(MORF2)_{1.2}$, or (iii) HSA-$(MORF2)_{9.4}$. Immediately after the addition of HSA-based samples, quantitative changes in the intracellular Ca^{2+} were monitored by flow cytometry at every 30s interval. To deplete cholesterol and inhibit CD20 crosslinking, cells were pre-incubated in the presence of β-CD (4%) for 20 min at 37°C. Tests were performed in triplicate for each sample.

2.6 Apoptosis Detection

Raji cells (2×10^5) were treated with Fab'-MORF1 (1μM, 1h)/HSA-$(MORF2)_x$ (1μM MORF2, 24 h, x= 0, 1.2, 5.4, 9.4, 16.6), GDC-0980 (0.4 μM, 24 h), or their combination. Afterward, cells were washed with PBS and stained with Annexin V-FITC and propidium

iodide (PI) in dark for 15 min, following the RAPID™ protocol provided by the manufacturer (Oncogene Research Products, Boston, MA).

2.7 Cytotoxicity Investigation

Raji cells (2×10^4) were suspended in 100 μL cell culture medium and seeded in 96-well plates. Then a same volume of cell culture medium containing a series of known concentrations of 800, 200, 50, 12.5, 3.125, 0.781, 0.195, 0.048, 0.0002, and 0 μM chemotherapeutics (GDC-0980, GEM, and DTX) were added. Meanwhile, Raji cells were also co-incubated with a constant concentration of KH-1, Fab'-MORF1 (1μM, 1h)/HSA-$(MORF2)_{9.4}$ (MORF2, 1μM). Cells were incubated at 37°C for 48 h. Then the CCK-8 solution (1:10) was added to each well and incubated for 3 h. The absorbance was measured using a microplate reader at 450 nm. Viability of chemo drugs treated cells was calculated as a percentage of the viability of untreated control. Viability of cells treated with drug + KH-1 was normalized based on the viability of KH-1 solely treated control.

2.8 Cell Cycle Evaluation

Raji cells (2×10^5) were treated with GDC-0980 (0.5 μM), GEM (0.5 μM), DTX (0.5 μM), and their combinations with KH-1, Fab'-MORF1 (1μM, 1h)/HSA-$(MORF2)_{9.4}$ (MORF2, 1μM) for 24 h. Then cells were washed with PBS and fixed by 70% ethanol at 4 °C overnight. Afterwards, cell pellets were washed by PBS and incubated with 50 μL RNase A (100 μg/mL) at 37 °C for 30 min. Then, 200 μL of PI (50 μg/mL) was added and co-incubated with cells at room temperature for 20 min before flow cytometry analysis.

2.9 Immunofluorescence Staining

Raji cells (2×10^5) were treated with: (i) cell culture medium (untreated); (ii) GDC-0980 (0.4 μM, 24 h); (iii) KH-1: Fab'-MORF1 (1μM, 1h)/HSA-$(MORF2)_{9.4}$ (1μM MORF2, 24 h); or (iv) GDC-0980 and KH-1 combination. After washed with PBS, cells were sequentially fixed by 4% paraformaldehyde for 15 min at room temperature, permeabilized by 90% methanol for 30 min on ice and stained with fluorescent labeled antibodies in 0.5% bovine serum albumin buffer for 1h at room temperature. Alexa Fluor 647 conjugated NF-κB p65 mAb, Alexa Fluor 488 conjugated Phospho-Bcl-2 (Ser70) (5H2) mAb, Alexa Fluor 488 conjugated Bax mAb, Alexa Fluor 488 conjugated P-Akt (T308) (D25E6) mAb, Alexa Fluor647 conjugated P-S6 (S235/235) (D57.2.2E) mAb, and Alexa Fluor647 conjugated P-Akt (S473) (D9E) mAb, obtained from Cell Signaling Technology, were used to detect the expression of NF-κB, Bcl-2, Bax, phospho-Akt (Thr 308, PI3K downstream), phospho-S6 (Ser 235/236, mTOR1 downstream), and phospho-Akt (Ser 473, mTOR2 downstream), respectively. After staining, cells were washed and fluorescence intensity within the cells was quantified by flow cytometry.

2.10 Caspase 3 Activation Study

After the treatments, Raji cells were washed with PBS andanalyzed for caspase-3 activity following the manufacturer's protocol provided by hi-PhiLux kit (OncoImmunin, Gaithersburg, MD).

2.11 Mitochondrial Membrane Potential Study

Mitochondrial depolarization was assessed by JC-1 mitochondrial membrane potential sensor (Thermo Scientific). After the treatments, 2×10^5 Raji cells were washed with PBS and resuspended in 200 μL PBS containing 4 μM JC-1 for 30 min at 37 °C. After washed with PBS, cells were analyzed by flow cytometry using 488 nm excitation with 530/30 nm and 585/42 nm band-pass filters. To the positive control, 0.5mM carbonyl cyanide *m*-chlorophenylhydrazone was co-incubated with JC-1 for 30 min before flow analysis.

3. Results and Discussion

3.1 Characterization of KH-1

The schematic synthesis routes of Fab'-MORF1 and HSA-$(MORF2)_x$ are shown in Figure 1A, B. Fab'-MORF1 was synthesized and characterized (Figure 1C), according to previously published methods [22-24]. The surface of HSA was functionalized with maleimide and further conjugated with freshly reduced MORF2 (3'-primary terminated with thiol group) via the thioether linkages with the feeding molar ratios of 1:2, 1:10, 1:20, and 1:30, to obtain the HSA-$(MORF2)_x$ with different valences (Figure 1B). The actual MORF2 valence in fabricated HSA-$(MORF2)_x$ was 1.2, 5.4, 9.4, and 16.6, respectively, as determined by UV spectroscopy (for MORF2) and BCA assay (for HSA). As confirmed in Figure 1D and Figure S1, the peaks shifted toward smaller elution volumes as molecular weight increased with increased valence.

Then the MORF1-MORF2 hybridizations were further investigated (Figure 1E). When the same MORF functionalized HSA-$(MORF2)_{9.4}$ and Fab'-MORF2 were premixed with equal MORF concentration at room temperature for 10 min, the size-exclusion chromatography only showed two separated peaks of HSA-$(MORF2)_{9.4}$ and Fab'-MORF2, respectively, thus ruling out the interaction between HSA and Fab'. After Fab'-MORF1 was premixed with HSA-$(MORF2)_{1.2}$, an apparent increase in molecular weight was observed. The peak further shifted to the column volume limit (~8 mL) when the valence of HSA-$(MORF2)_x$ increased to 9.4. These results indicated that HSA-$(MORF2)_x$ could indeed hybridize with Fab'-MORF1 through the complementary MORF1-MORF2 hybridization. Moreover, the higher valence of HSA-$(MORF2)_x$ enables greater capacity to simultaneously crosslink a higher number of Fab'-MORF1, which is important for improving the crosslinking efficiency of cell surface CD20.

3.2 Surface CD20 Crosslinking Translates into Apoptosis

To elucidate the relationship between extracellular receptor actuation and intracellular signal activation, KH-1-mediated CD20 crosslinking and calcium influx were determined. Surface CD20 is considered non-internalizing and functions as a store-operated calcium channel [31]. Clustering of CD20 can result in significant CD20 internalization and triggers an intracellular signaling response characterized by a rapid rise in cytosolic calcium [23, 26, 32].

When highly CD20 expressing Raji cells were consecutively treated with Fab'-MORF1-Cy5 and HSA-mal-Cy3 (Figure 2A), cell surface was decorated with strong Cy5 fluorescence but

barely visible Cy3 fluorescence. In consistence, majority of Fab'-MORF1-Cy5 only extracellularly bound and remained on the cell membrane, as the exposure to proteinase K considerably decreased the Cy5 positive cells from ~85% to ~10%. Moreover, no FRET signal between Cy3 and Cy5 was observed either before or after CD20 enzymatic digestion. Due to the absence of CD20 crosslinking, no response in intracellular calcium concentration was observed (Figure 2B).

By comparison, when Raji cells were consecutively treated with Fab'-MORF1-Cy5 and HSA-$(MORF2)_{1.4}$-Cy3 (Figure 2C), both Cy5 and Cy3 fluorescence formed surface-bound ring patterns around the targeted cells, and substantially co-localized, demonstrating MORF1-MORF2 hybridization. After surface CD20 enzymatic digestion, most of the cells that had been dual Cy5/Cy3 stained became dual negative. Similarly, the originally apparent FRET signal disappeared after CD20 digestion. Thus, merely binding or assembly at surface CD20 was not sufficient to initiate CD20 crosslinking and subsequent internalization. Consequently, calcium influx was not triggered (Figure 2D).

In contrast, a significant internalization and co-localization of Cy5 and Cy3 fluorescence inside cells was seen after Raji cells were consecutively treated with Fab'-MORF1-Cy5 and HSA-$(MORF2)_{11.4}$-Cy3 (Figure 2E).This was further confirmed by a great proportion of dual dye positive cells and the intracellular FRET signal still remaining after surface CD20 enzymatic removal, thereby verifying that multivalent binding of CD20-pretargeted Fab'-MORF1 by high valence of HSA-$(MORF2)_x$ was required to trigger CD20 crosslinking. Notably, the intracellular signal, calcium influx, was switched on in response to the Fab'-MORF1→HSA-$(MORF2)_{9.4}$ treatment (Figure 2F). Moreover, when the cells were pretreated with β-CD that blocked CD20 crosslinking [23, 33], KH-1-mediated calcium influx was also inhibited, further confirming the intracellular signal activation was translated from extracellular receptor crosslinking.

We next determined the optimal valence of KH-1 to initiate intracellular apoptosis response (Figure 2G). In contrast to KH-1 (valence=0, and 1.2), which only triggered moderate apoptosis, KH-1 with higher valences of 5.4, 9.4 and 16.6 significantly enhanced apoptosis, highlighting the importance of multivalence. KH-1 (v=5.4) exhibited slightly better effect than rituximab (RTX) crosslinked by goat anti-human (GAH) secondary antibody. Meanwhile, although KH-1 (v=9.4) resulted in markedly enhanced apoptosis as compared with KH-1 (v=5.4), continuously increasing the valence to 16.6 did not further increase the overall apoptosis. These results suggested the valence of 9.4 in KH-1 might be optimal, as KH-1 with lower valence of 5.4 was less efficient in crosslinking or multimerization of CD20 while the extra MORF2 on albumin in KH-1 with higher valence of 16.6 might not be operative and accessible to interact with the surface-bound Fab'-MORF1 for subsequent CD20 crosslinking.

3.3 KH-1 Acts as Chemo Sensitizer

To determine whether KH-1-mediated transduction of extracellular actuation to intracellular signal could sensitize cancer cells to chemotherapeutic agents, drugs with distinct mechanisms of action were selected to combine with KH-1 to treat Raji cells (Figure 3). Cell viability studies illustrated that the cytotoxicities of docetaxel (DTX, microtubulestabilizer,

Figure 3A), gemcitabine (GEM, nucleoside analogue, Figure 3B), and GDC-0980 (PI3K/mTOR inhibitor, Figure 3C) were potentiated in the presence of KH-1. As these drugs have different effects on inhibition of cell cycle with G2/M phase arrest by DTX [14], S phase arrest by GEM [34], and G1/G0 arrest by GDC-0980 [35], we further investigated the impact of KH-1 on drug-modulated cell cycle. Interestingly, while KH-1 alone had little impact on cell cycle regulation, it exerted drug-dependent effect on the alteration of cell cycle when combined with different drugs (Figure 3D): KH-1 enhanced DTX-induced G2/M arrest, GEM-induced S phase arrest and GDC-0980-induced G1/G0 arrest. Notably, these results might suggest the following facts: (1) the ability of KH-1 to potentiate the drug efficacy did not rely on a specific type of drug; (2) thus, KH-1 might sensitize cancer cell to a broad spectrum of cytotoxic agents; and (3) the mechanisms underlying the increased cell susceptibility to different drugs might share universal pathways effected by KH-1.

3.4 KH-1 Inhibits Survival Pathways

Our results with KH-1-mediated chemosensitization showed general applicability to various cytotoxic drugs, suggesting the threshold for cell susceptibility might be decreased due to the perturbation of the intracellular survival signaling. To explain this, we chose GDC-0980 as the combinatory agent with KH-1, and assessed their separate and joint effects on the regulation of pivotal cell survival signaling molecules.

We first investigated signaling components of the PI3K/Akt/mTOR network (Figure 4 A-C). The combination treatment elicited a strong inhibition across all the tested downstream biomarkers of PI3K (phospho-AktThr 308), mTOR1 (phospho-S6), and mTOR2 (phospho-Akt Ser473). As a potent dual inhibitor of PI3K/mTOR, GDC-0980 played a dominant role in the down-regulation of PI3K and mTOR1. Although the inhibition of mTOR2 induced by GDC-0980 alone was not as significant as PI3K or mTOR1, further addition of KH-1 markedly decreased mTOR2 activity. NF-κB signaling, another well-known survival pathway that suppresses apoptosis and is also a feedback mechanism triggered by PI3K/AKT/mTOR inhibition [36], was assessed. Both GDC-0980 and KH-1 inhibited NF-κB to some degree, but the lowest level of NF-κB occurred when they were combined (Figure 4D). Identically, their combination also resulted in the most potent activation of pro-apoptotic protein Bax (Figure 4E) and concomitant deactivation of anti-apoptotic protein Bcl-2 (Figure 4F).

The function of Akt is to stimulate cell growth, and simultaneously suppress cell death. It is activated downstream from PI3K, and has a primary effector mTOR [37, 38]. mTOR can be characterized by two complexes: mTOR1 that controls S6K phosphorylation leading to protein synthesis, and mTOR2 that controls Ser473 phosphorylation of Akt (Figure 4G). While GDC-0980 potently inhibited PI3K and mTOR1, it had lesser efficacy in regulating mTOR2. However, the participation of KH-1 potentiated the GDC-0980-mediated inhibition of mTOR2, thereby catalyzing full deactivation of Akt. In addition, GDC-0980 and KH-1 also worked together to down-regulate NF-κB and Bcl-2 which are broadly associated with oncogenesis through their ability to facilitate cell progression. These results supported previous finding [39,40] that the engagement of CD20 receptor negatively regulates the

MAPK/mTOR/ NF-κB and Bcl-2/Bax pathways, and suggested KH-1 was valid to augment chemotherapy through inhibiting cell survivals.

3.5 KH-1 Enhances Apoptosis Pathways

Next, we examined whether greater efficacy from the combined treatment involved enhanced apoptosis. As indicated in Figure 5A, GDC-0980 did not enhance or interfere with KH-1-mediated CD20 crosslinking. In contrast, GDC-0980 apparently negated the calcium influx induced by KH-1 (Figure 5B), which might be explained by PI3K-dependent extracellular calcium influx [39] and potential inhibition of calcium influx by PI3K inhibitors such as GDC-0980. As calcium influx is one of the most important mechanisms underlying the effectiveness of CD20 crosslinking function [23], whether GDC-0980 that abrogated calcium influx antagonized KH-1 in apoptosis was investigated. Of note, Figure 5C showed a significant improvement in early apoptosis when they were combined. This result is in consistence with the cytotoxicity study that GDC-0980 + KH-1 drastically outperformed GDC-0980 alone. Presumably, the abrogation of calcium influx by GDC-0980 could be compensated by other pathways.

Caspase-3 is a crucial mediator and executioner of apoptosis. We discovered that GDC-0980 and KH-1 could cooperate to promote caspase-3 activation (Figure 5D). In particular, their combinatorial effect could be partially inhibited by the pretreatment with β-CD (CD20 crosslinking inhibitor), but not EGTA (calcium chelating agent). This result provides evidence that KH-1-mediated CD20 crosslinking triggered another apoptotic cascade that bypassed the GDC-0980-caused loss of calcium influx signaling. Given that mitochondrial pathway is one of major effector mechanisms for CD20 crosslinking [22,23] and is responsible for the observed alteration in Bcl-2/Bax ratio and caspase-3 activation in this study, mitochondrial depolarization was thus investigated (Figure 5E). Indeed, co-delivery of GDC-0980 and KH-1 induced more potent decrease in mitochondrial membrane potential (MMP) than any of them used alone. Collectively, these results suggested KH-1 could also leverage the potentiation of apoptotic signaling to elicit chemosensitization.

3.6 Internalization and Subcellular Trafficking of KH-1: Implication for Fab'-MORF1/HSA-$(MORF2)_x$-Drug System

To validate the relevance of KH-1 system as a potential intracellular delivery vehicle for anticancer agents, we examined the effects of pretargeting and multivalent binding on cell internalization (Figure 6A). In the absence of Fab'-MORF1, HSA-$(MORF2)_{11.4}$-Cy3 was mostly precluded from cells, due to the macromolecular size of HSA and its poor membrane affinity [28]. Meanwhile, exposure of Fab'-MORF1 pretargeted Raji cells to HSA-$(MORF2)_{1.4}$-Cy3 only resulted in its extracellular binding to cell surface. However, substantial internalization and lysosomal localization of albumin was observed after consecutive treatment of Fab'-MORF1 and HSA-$(MORF2)_{11.4}$-Cy3, thereby emphasizing the indispensable roles of both pretargeting and multivalency in regulating intracellular targeted delivery. Moreover, the effects of the time lag between the pretargeting and secondary step targeting on the accessibilities of surface-bound Fab'-MORF1 to the multivalent crosslinking reagent HSA-(MORF2)11.4-Cy3 have been investigated and

discussed (Figure S2). Even after a 5 h time lag between the administrations of the two nanoconjugates high levels of apoptosis were detected.

HSA has been extensively demonstrated as promising drug vector for cancer therapy, because of its versatile attributes such as good biocompatibility, long blood circulation, easy scale-up, and its capability to load a wide range of drugs through non-covalent complex formation or covalent surface attachment [27]. As a result, HSA-based therapeutics (*e.g.* Abraxane®) are clinically available. However, HSA has also been found to have very poor cell internalization efficiency, thus resulting in sublethal intracellular drug concentration. Consequently, despite multiple significant advantages, Abraxane® is still found to induce drug resistance [42, 43]. With the receptor pretargeting and crosslinking attributes, the KH-1 system is expected to be more effective at delivering covalently attached drugs intracellularly. Given that neonatal Fc receptor (FcRn) is responsible for the HSA half-life extension by a mechanism of binding HSA in the acidic endosomal compartments, recycling to the extracellular surface, and returning HSA back to bloodstream [44, 45], there is concern that surface modification of HSA might negatively introduce conformational change or steric hindrance that disrupts interaction with FcRn and decrease the circulatory half-life of HSA-based system [46]. Whether the conjugation of MORF2 and attachment of drugs would affect the HSA blood circulation is not known and certainly needs to be assessed in the future study.

As above, our results supported further development of Fab'-MORF1/HSA-$(MORF2)_x$-drug system that simultaneously integrates chemosensitization function and intracellularly targeted drug delivery, which is an underexplored area in the field of nanomedicine. To verify the hypothesis, the anthracycline anticancer drug, epirubicin (EPI), was covalently conjugated to HSA as previously described [29, 30]. The characterizations of HSA-EPI and HSA-$(MORF2)_x$-EPI are shown in Figure 6B. As expected, Fab'-MORF1/ HSA-$(MORF2)_x$-EPI mediated significantly improved cell uptake of EPI (Figure 6C) and superior cytotoxicity (Figure 6D) as compared with HSA-EPI.

In terms of chemosensitization, an ideal strategy should avoid its own additional toxicity, easily access to its target and be broadly applicable to various toxic drugs. Fab'-MORF1/ HSA-$(MORF2)_x$ system can meet all these three criteria because (1) it is a drug-free system; (2) it is a pretargeting two-step process that triggers extracellular functions; and (3) it can initiate the inhibition or activation of multiple innate signaling pathways that increase cell susceptibility to apoptosis. Moreover, the transduction of surface receptor crosslinking to chemosensitization is also accompanied by the intracellular internalization of the HSA-based system, alongside the covalently conjugated chemotherapeutics. In this way, intracellular drug delivery and chemosensitization could be orchestrated and achieved simultaneously in the same cell and using one single system (Figure 6E).

In the present mechanism study, the *in vitro* results support the proof-of-concept that leveraging surface receptor crosslinking elicits chemosensitization, which differs from conventional strategies to enhance cancer cell susceptibility to chemo drugs. Of note, *in vivo* environment is quite different from the *in vitro* cell culture and there is a need to overcome even more complicated physiology barriers. Thus, future directions will be focused on

investigating the feasibility for *in vivo* applications, finding unexpected challenges in animals, and optimizing the treatment (e.g., nanoconjugate structure and treatment regimen) to enhance therapeutic efficacy.

4. Conclusions

In summary, we have rationally developed a drug-free HSA-based therapeutics to promote cancer cell sensitivity to cytotoxic drugs. Multivalent binding of CD20 receptor-bound Fab'-MORF1 afforded by HSA-$(MORF2)_x$ efficiently triggers extracellular CD20 clustering, and subsequently sensitizes cancer cell to different drugs with distinct mechanisms of action. The increased cell susceptibility is due to the significant transduction of extracellular receptor crosslinking input into intracellular output of simultaneous survival pathway inhibition and apoptotic pathway augmentation. Moreover, substantial internalization and lysosomal localization of the albumin were observed after the engagement of KH-1-triggered CD20 crosslinking. When EPI was covalently conjugated to KH-1, EPI-loaded KH-1 exhibited improved drug uptake and enhanced cytotoxicity as compared with HSA-EPI, thus integrating both targeted intracellular drug delivery and chemosensitization function within one single system.

Supplementary Material

Refer to Web version on PubMed Central for supplementary material.

Acknowledgments

The work was supported in part by NIH grant RO1 GM95606 (to J.K.) from the National Institute of General Medical Sciences, Huntsman Cancer Institute, and University of Utah Research Foundation. S.S. thanks the Thailand Research Fund for support through the Royal Golden Jubilee Ph.D. program (grant PHD/0139/2557). We acknowledge support of funds in conjunction with grant P30 CS042014 awarded to Huntsman Cancer Institute and to the ET Program at Huntsman Cancer Institute.

References

[1]. Jin F, Wang Y, Li M, Zhu Y, Liang H, Wang C, Wang F, Zhang CY, Zen K, Li L, MiR-26 enhances chemosensitivity and promotes apoptosis of hepatocellular carcinoma cells through inhibiting autophagy, Cell Death Dis. 8 (2017) e2540. [PubMed: 28079894]

[2]. Liu T, Xiong J, Yi S, Zhang H, Zhou S, Gu L, Zhou M, FKBP12 enhances sensitivity to chemotherapy-induced cancer cell apoptosis by inhibiting MDM2, Oncogene 36 (2017) 1678–1686. [PubMed: 27617579]

[3]. Li M, Zhang Z, Hill DL, Wang H, Zhang R, Curcumin, a dietary component, has anticancer, chemosensitization, and radiosensitization effects by down-regulating the MDM2 oncogene through the PI3K/mTOR/ETS2 pathway, Cancer Res. 67 (2007) 1988–1996. [PubMed: 17332326]

[4]. Zhou BB, Bartek J, Targeting the checkpoint kinases: chemosensitization versus chemoprotection, Nat. Rev. Cancer 4 (2004) 216–225. [PubMed: 14993903]

[5]. Wang S, El-Deiry WS, Requirement of p53 targets in chemosensitization of colonic carcinoma to death ligand therapy, Proc. Natl. Acad.Sci. U. S.A. 100 (2003) 15095–15100. [PubMed: 14645705]

[6]. Nervi B, Ramirez P, Rettig MP, Uy GL, Holt MS, Ritchey JK, Prior JL, Piwnica-Worms D, Bridger G, Ley TJ, DiPersio JF, Chemosensitization of acute myeloid leukemia (AML) following

mobilization by the CXCR4 antagonist AMD3100, Blood 113 (2009), 6206–6214. [PubMed: 19050309]

[7]. Gandhi NS, Tekade RK, Chougule MB, Nanocarrier mediated delivery of siRNA/miRNA in combination with chemotherapeutic agents for cancer therapy: current progress and advances, J. Control. Release 194 (2014) 238–256. [PubMed: 25204288]

[8]. Szakécs G, Paterson JK, Ludwig JA, Booth-Genthe C, Gottesman MM, Targeting multidrug resistance in cancer, Nat. Rev. Drug Discov 5 (2006) 219–234. [PubMed: 16518375]

[9]. Longley DB, Johnston PG, Molecular mechanisms of drug resistance, J. Pathol. 205 (2005) 275–292. [PubMed: 15641020]

[10]. Ramos P, Bentires-Alj M, Mechanism-based cancer therapy: resistance to therapy, therapy for resistance, Oncogene 34 (2015) 3617–3626. [PubMed: 25263438]

[11]. Whitehead KA, Langer R, Anderson DG, Knocking down barriers: advances in siRNA delivery, Nat. Rev. Drug Discov. 8 (2009) 129–138. [PubMed: 19180106]

[12]. Barua S, Mitragotri S, Challenges associated with penetration of nanoparticles across cell and tissue barriers: a review of current status and future prospects, Nano Today 9 (2014) 223–243. [PubMed: 25132862]

[13]. Li L, Sun W, Zhong J, Yang Q, Zhu X, Zhou Z, Zhang Z, Huang Y, Multistage nanovehicle delivery system based on stepwise size reduction and charge reversal for programmed nuclear targeting of systemically administered anticancer drugs, Adv. Funct. Mater. 25 (2015) 4101–4113.

[14]. Li L, Sun W, Zhang Z, Huang Y. Time-staggered delivery of docetaxel and H1-S6A, F8A peptide for sequential dual-strike chemotherapy through tumor priming and nuclear targeting, J. Control. Release 232 (2016) 62–74. [PubMed: 27098443]

[15]. Arola OJ, Saraste A, Pulkki K, Kallajoki M, Parvinen M, Voipio-Pulkki LM, Acute doxorubicin cardiotoxicity involves cardiomyocyte apoptosis, Cancer Res. 60 (2000) 1789–1792. [PubMed: 10766158]

[16]. Spain L, Diem S, Larkin J, Management of toxicities of immune checkpoint inhibitors, Cancer Treat. Rev. 44 (2016) 51–60. [PubMed: 26874776]

[17]. Mannix RJ, Kumar S, Cassiola F, Montoya-Zavala M, Feinstein E, Prentiss M, Ingber DE, Nanomagnetic actuation of receptor-mediated signal transduction, Nat. Nanotechnol. 3 (2008) 36–40. [PubMed: 18654448]

[18]. Mitchell MJ, Webster J, Chung A, Guimarães PP, Khan OF, Langer R, Polymeric mechanical amplifiers of immune cytokine-mediated apoptosis, Nat. Commun 8 (2017) 14179. [PubMed: 28317839]

[19]. Wu K, Liu J, Johnson RN, Yang J, Kopeček J, Drug-free macromolecular therapeutics: induction of apoptosis by coiled-coil-mediated cross-linking of antigens on the cell surface, Angew. Chem. Int. Ed. 49 (2010) 1493–1497.

[20]. Graves JD, Kordich JJ, Huang TH, Piasecki J, Bush TL, Sullivan T, Foltz IN, Chang W, Douangpanya H, Dang T, O'Neill JW, Apo2L/TRAIL and the death receptor 5 agonist antibody AMG 655 cooperate to promote receptor clustering and antitumor activity, Cancer Cell 26 (2014) 177–189. [PubMed: 25043603]

[21]. Riley RS, Day ES, Frizzled7 antibody-functionalized nanoshells enable multivalent binding for wnt signaling inhibition in triple negative breast cancer cells. Small 13 (2017) 1700544.

[22]. Li L, Yang J, Wang J, Kopeček J, Amplification of CD20 cross-linking in rituximab-resistant B-lymphoma cells enhances apoptosis induction by drug-free macromolecular therapeutics, ACS Nano 12 (2018) 3658–3670. [PubMed: 29595951]

[23]. Li L, Yang J, Wang J, Kopeček J, Drug-free macromolecular therapeutics induce apoptosis *via* calcium influx and mitochondrial signaling pathway, Macromol. Biosci 18 (2018) 1700196.

[24]. Chu TW, Yang J, Zhang R, Sima M, Kopeček J, Cell surface self-assembly of hybrid nanoconjugates via oligonucleotide hybridization induces apoptosis, ACS Nano 8 (2014) 719–730. [PubMed: 24308267]

[25]. Kaplan-Lefko PJ, Graves JD, Zoog SJ, Pan Y, Wall J, Branstetter DG, Moriguchi J, Coxon A, Huard JN, Xu R, Peach ML, Conatumumab, a fully human agonist antibody to death receptor 5,

induces apoptosis via caspase activation in multiple tumor types, Cancer Biol. Ther. 9 (2010) 618–631. [PubMed: 20150762]

[26]. Zhang N, Khawli LA, Hu P, Epstein AL Generation of rituximab polymer may cause hyper-cross-linking-induced apoptosis in non-Hodgkin's lymphomas, Clin. Cancer Res. 11 (2005) 5971–5980. [PubMed: 16115941]

[27]. Kratz F, Albumin as a drug carrier: design of prodrugs, drug conjugates and nanoparticles, J. Control. Release 132 (2008) 171–183. [PubMed: 18582981]

[28]. Ichimizu S, Watanabe H, Maeda H, Hamasaki K, Nakamura Y, Chuang VT, Kinoshita R, Nishida K, Tanaka R, Enoki Y, Ishima Y, Design and tuning of a cell-penetrating albumin derivative as a versatile nanovehicle for intracellular drug delivery, J. Control. Release 277 (2018) 23–34. [PubMed: 29530390]

[29]. Choi SH, Byeon HJ, Choi JS, Thao L, Kim I, Lee ES, Shin BS, Lee KC, Youn YS, Inhalable self-assembled albumin nanoparticles for treating drug-resistant lung cancer, J. Control. Release 197 (2015) 199–207. [PubMed: 25445703]

[30]. Xu R, Fisher M, Juliano RL, Targeted albumin-based nanoparticles for delivery of amphipathic drugs, Bioconjugate Chem. 22 (2011) 870–878.

[31]. Janas E, Priest R, Wilde JI, White JH, Malhotra R, Rituxan (anti-CD20 antibody)-induced translocation of CD20 into lipid rafts is crucial for calcium influx and apoptosis, Clin. Exp. Immunology 139 (2005) 439–446.

[32]. Unruh TL, Li H, Mutch CM, Shariat N, Grigoriou L, Sanyal R, Brown CB, Deans JP, Cholesterol depletion inhibits src family kinase - dependent calcium mobilization and apoptosis induced by rituximab crosslinking, Immunology 116 (2005) 223–232. [PubMed: 16162271]

[33]. Hartley JM, Chu TW, Peterson EM, Zhang R, Yang J, Harris J, Kopeček J, Super-resolution imaging and quantitative analysis of membrane protein/lipid raft clustering mediated by cell-surface self-assembly of hybrid nanoconjugates, ChemBioChem 16 (2015) 1725–1729. [PubMed: 26097072]

[34]. Shi Z, Azuma A, Sampath D, Li YX, Huang P, Plunkett W, S-Phase arrest by nucleoside analogues and abrogation of survival without cell cycle progression by 7-hydroxystaurosporine, Cancer Res. 61 (2001) 1065–1072. [PubMed: 11221834]

[35]. Wallin JJ, Edgar KA, Guan J, Berry M, Prior WW, Lee L, Lesnick JD, Lewis C, Nonomiya J, Pang J, Salphati L, GDC-0980 is a novel class I PI3K/mTOR kinase inhibitor with robust activity in cancer models driven by the PI3K pathway, Mol. Cancer Ther. 10 (2011) 2426–2436. [PubMed: 21998291]

[36]. Dan HC, Cooper MJ, Cogswell PC, Duncan JA, Ting JP, Baldwin AS, Akt-dependent regulation of NF-κB is controlled by mTOR and Raptor in association with IKK, Genes Dev. 22 (2008) 1490. [PubMed: 18519641]

[37]. Engelman JA, Targeting PI3K signalling in cancer: opportunities, challenges and limitations, Nat. Rev. Cancer 9 (2009) 550–562. [PubMed: 19629070]

[38]. Mizrachi A, Shamay Y, Shah J, Brook S, Soong J, Rajasekhar VK, Humm JL, Healey JH, Powell SN, Baselga J, Heller DA, Tumour-specific PI3K inhibition via nanoparticle-targeted delivery in head and neck squamous cell carcinoma, Nat. Commun 8 (2017) 14292. [PubMed: 28194032]

[39]. Jazirehi AR, Bonavida B, Cellular and molecular signal transduction pathways modulated by rituximab (rituxan, anti-CD20 mAb) in non-Hodgkin's lymphoma: implications in chemosensitization and therapeutic intervention, Oncogene 24 (2005) 2121–2143. [PubMed: 15789036]

[40]. Leseux L, Laurent G, Laurent C, Rigo M, Blanc A, Olive D, Bezombes C, PKC ζ–mTOR pathway: a new target for rituximab therapy in follicular lymphoma, Blood 111 (2008) 285–291. [PubMed: 17855629]

[41]. Kansra V, Groves C, Gutierrez-Ramos JC, Polakiewicz RD, Phosphatidylinositol 3-kinase-dependent extracellular calcium influx is essential for CX3CR1-mediated activation of the mitogen-activated protein kinase cascade, J. Biol. Chem. 276 (2001) 31831–31838. [PubMed: 11432847]

[42]. Chen Q, Liang C, Wang C, Liu Z, An imagable and photothermal “abraxane-like” nanodrug for combination cancer therapy to treat subcutaneous and metastatic breast tumors, Adv.Mater. 27 (2015) 903–910. [PubMed: 25504416]

[43]. Zhao M, Lei C, Yang Y, Bu X, Ma H, Gong H, Liu J, Fang X, Hu Z, Fang Q, Abraxane, the nanoparticle formulation of paclitaxel can induce drug resistance by up-regulation of P-gp, PLoS One 10 (2015) e0131429. [PubMed: 26182353]

[44]. Sockolosky JT, Szoka FC, The neonatal Fc receptor, FcRn, as a target for drug delivery and therapy, Adv. Drug Deliver. Rev 91 (2015) 109–124.

[45]. Larsen MT, Kuhlmann M, Hvam ML, Howard KA, Albumin-based drug delivery: harnessing nature to cure disease, Mol. Cell.Ther. 4 (2016) 3. [PubMed: 26925240]

[46]. Petersen SS, Kläning E, Ebbesen MF, Andersen B, Cameron J, Sørensen ES, Howard KA, Neonatal Fc receptor binding tolerance toward the covalent conjugation of payloads to cysteine 34 of human albumin variants, Mol. Pharmaceutics 13 (2015) 677–682.

Highlights

- Human serum albumin-based therapeutic (KH-1) sensitizes cancer cells to various chemo drugs via inhibiting survival pathway and augmenting apoptotic pathway.
- Surface receptor crosslinking can be leveraged to elicit chemosensitization effect.
- KH-1 and drug combination represents therapeutic advantage in cancer treatment.

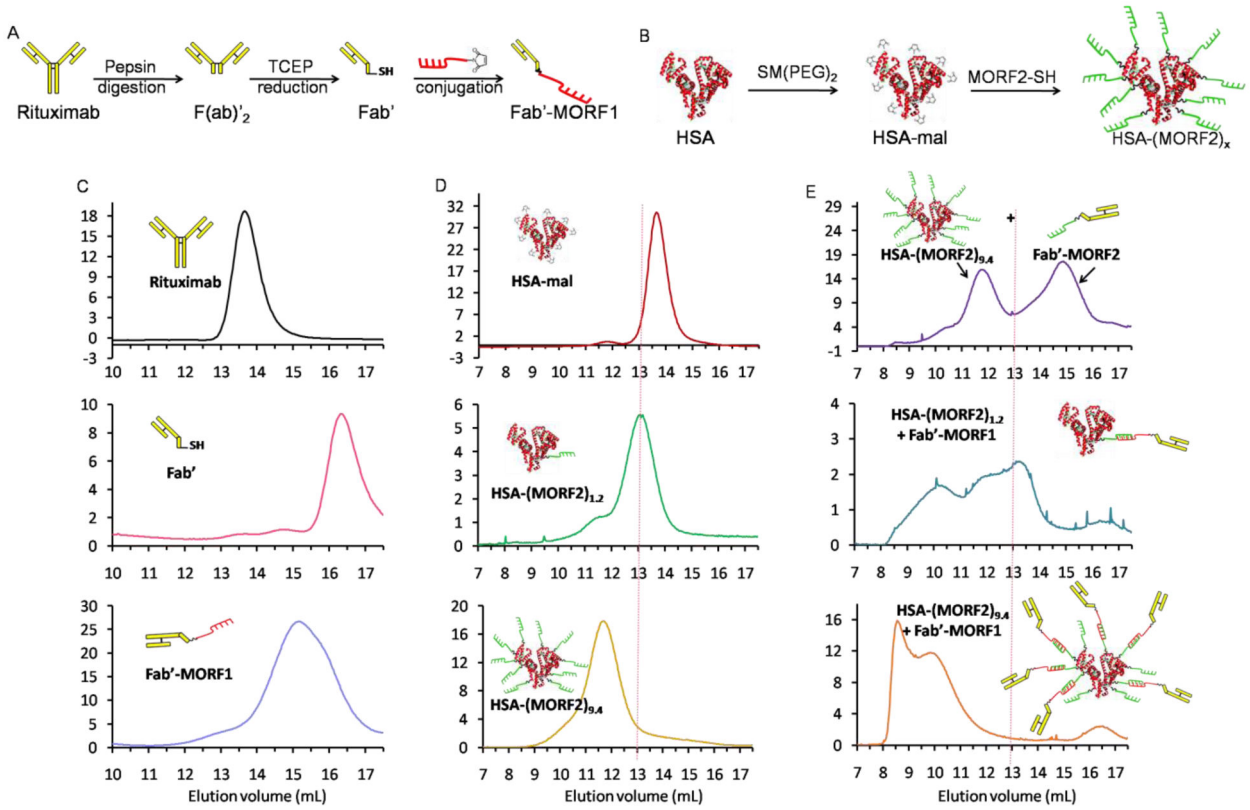

Figure 1.

Schematic illustrations of synthesis of (A) Fab'-MORF1 and (B) HSA-$(MORF2)_X$. Size-exclusion chromatography characterization of (C) Fab'-MORF1, (D) HSA-$(MORF2)_X$, and (E) their 1:1 MORF mixture after being incubated at room temperature for 10 min, using Sephacryl S-200column eluted with phosphate buffered saline (PBS, pH 7.4) with flow rate of 0.4 mL/min, detected at 280 nm.

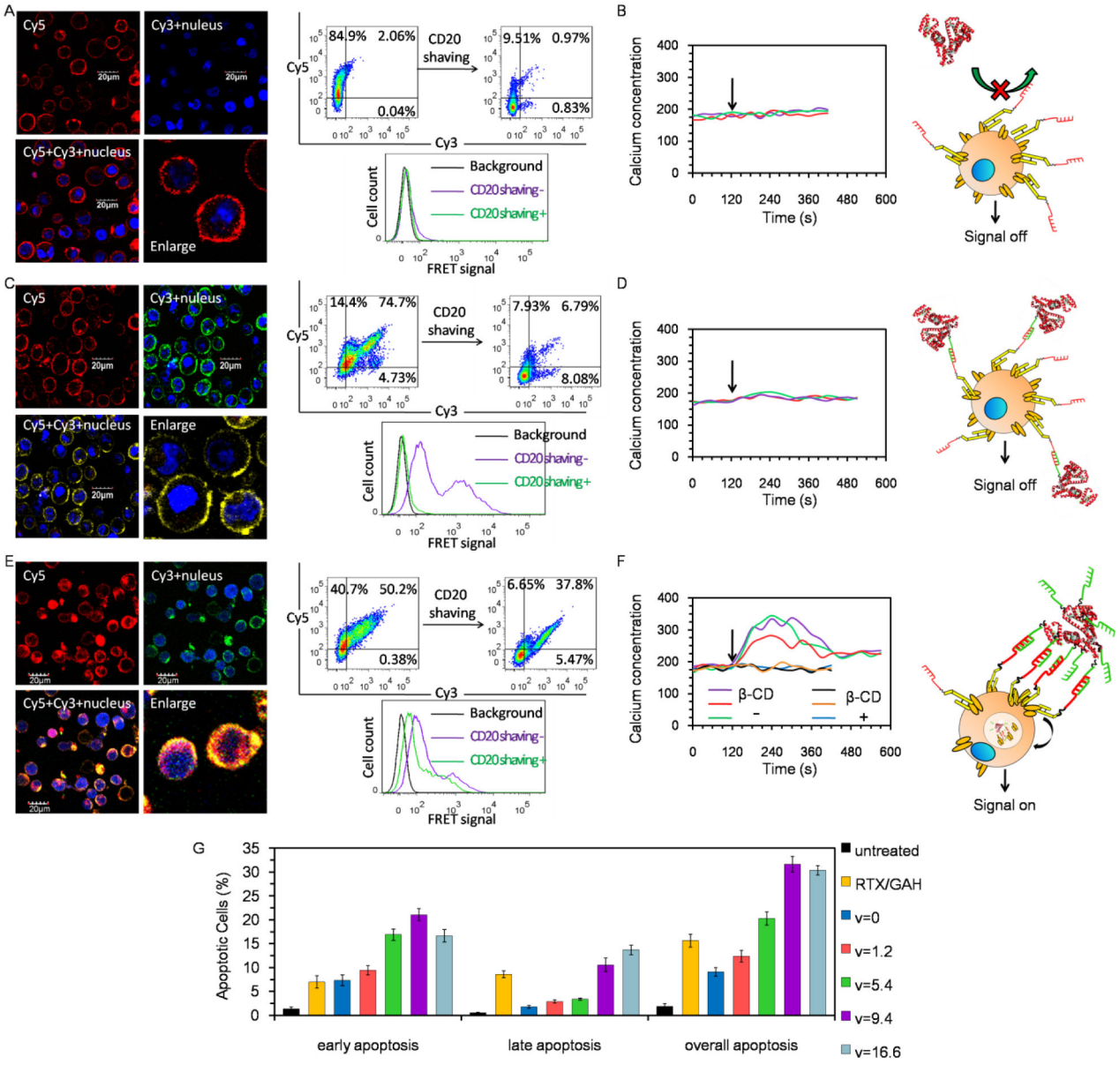

Figure 2.

CD20 crosslinking activities and calcium influx induction after Fab'-MORF1 pretargeted Raji cells were treated with (A, B) HSA-mal, (C,D) HSA-MORF2, and (E, F) HSA-$(MORF2)_x$ with high valence. (A, C, E) CD20 highly expressing Raji cells were exposed to Fab'-MORF1-Cy5 (1 μM MORF1, 1 h), and then further treated with (A) HSA-mal-Cy3 (1 μM HSA, 5 h), (C) HSA-$(MORF2)_{1.4}$-Cy3 (1 μM MORF2, 5 h), or (E) HSA-$(MORF2)_{11.4}$-Cy3 (1 μM MORF2, 5 h). Afterward, cell nuclei were stained with Hoechst 33342, and cells were visualized under confocal microscopy. Red: Cy5; Green: Cy3; Blue: nucleus. Meanwhile, surface CD20 receptors of treated cells were enzymatically digested by proteinase K. Flow cytometry was applied to detect the Cy3, Cy5 and their FRET signal before and after CD20 digestion. (B, D, F) Time-dependent change in intracellular Ca^{2+} as determined by flow cytometry-based quantification of Fluo-3AM fluorescence intensity.

Raji cells, pretreated with Fab'-MORF1 and loaded with Fluo-3AM, were excited at 488 nm and the emission at 530 nm was measured on flow cytometry. A baseline was obtained for 120 s before stimulation with (B) HSA-mal, (D) HSA-$(MORF2)_{1.2}$, (F) HSA-$(MORF2)_{9.4}$ crosslinking (indicated by black arrow).To deplete cholesterol and inhibit CD20 crosslinking, cells were pre-incubated 20 min at 37°C in the presence of β-CD (β-cyclodextrin). (G) Apoptosis induction after Raji cells were consecutively treated with Fab'-MORF1 (1 μM MORF1, 1 h) and HSA-$(MORF2)_x$ (1 μM MORF2, 18 h, x=0, 1.2, 5.4, 9.4, 16.6). Then cells were washed with PBS, followed by the AnnexinV-FITC/PI double staining and flow cytometry analysis. Cells that were not treated or treated with RTX (0.5 μM, 1 h)/GAH (0.5 μM, 18 h) were set as controls.

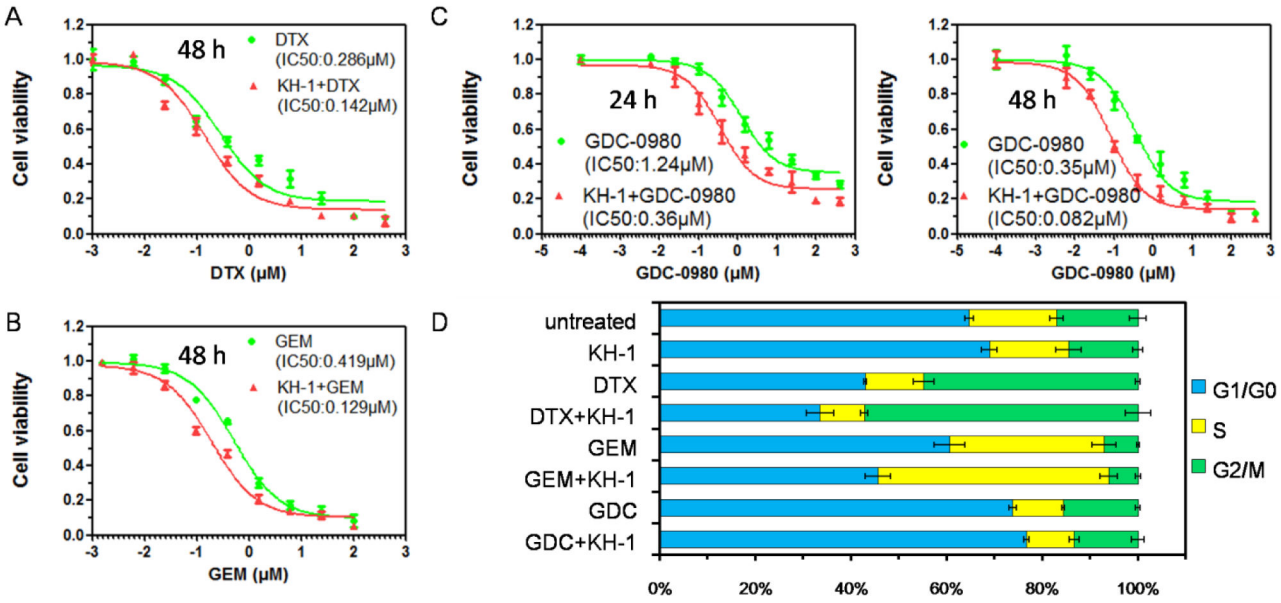

Figure 3.

Viabilities of Raji cells after co-incubation with Fab'-MORF1 (1μM, 1h)/HSA-$(MORF2)_{9.4}$ (MORF2, 1μM) and a series of known concentrations of (A) docetaxel (DTX), (B) gemcitabine (GEM), and (C) GDC-0980 for 24 h or 48 h. Viability of drugs treated cells was calculated as a percentage of the viability of untreated control. Viability of cells treated with drug + KH-1 was normalized based on the viability of KH-1 solely treated control.

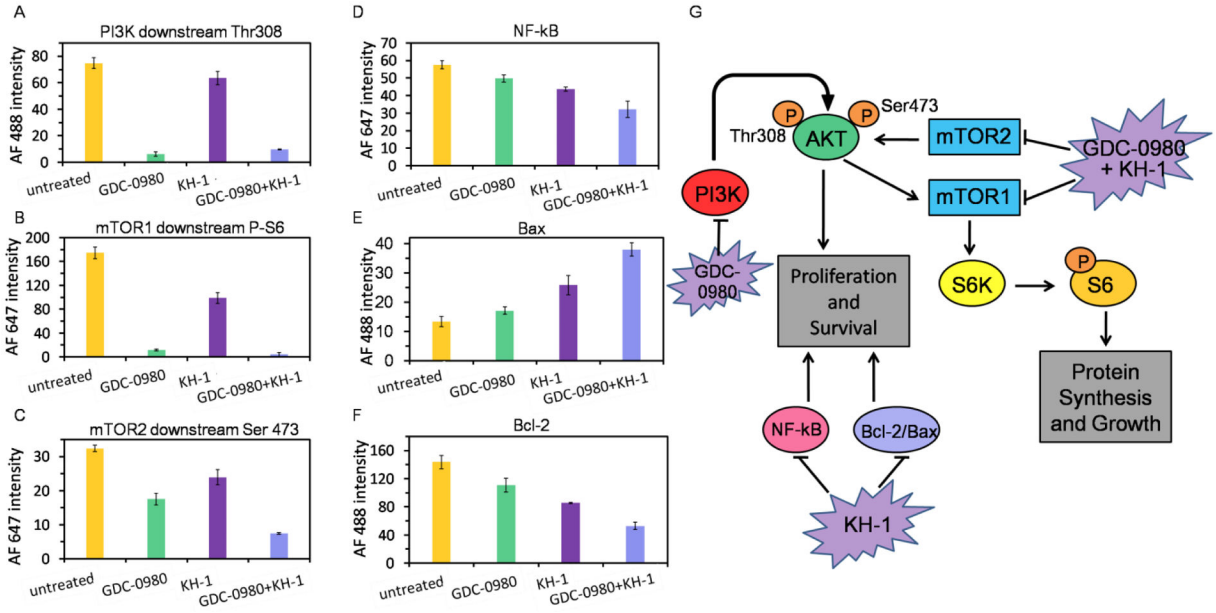

Figure 4.

Expression of (A) phospho-Akt (Thr308), (B) phospho-S6, (C) phospho-Akt (Ser473), (D) NF-κB, (E) Bax, (F) Bcl-2 in Raji cells following treatment with GDC-0980 (0.4 μM, 24 h), KH-1 Fab'-MORF1 (1μM, 1h)/HSA-$(MORF2)_{9.4}$ (1μM MORF2, 24 h), or their combination. (G) Schematic illustration of survival pathway inhibition by the combination therapy of GDC-0980 and KH-1.

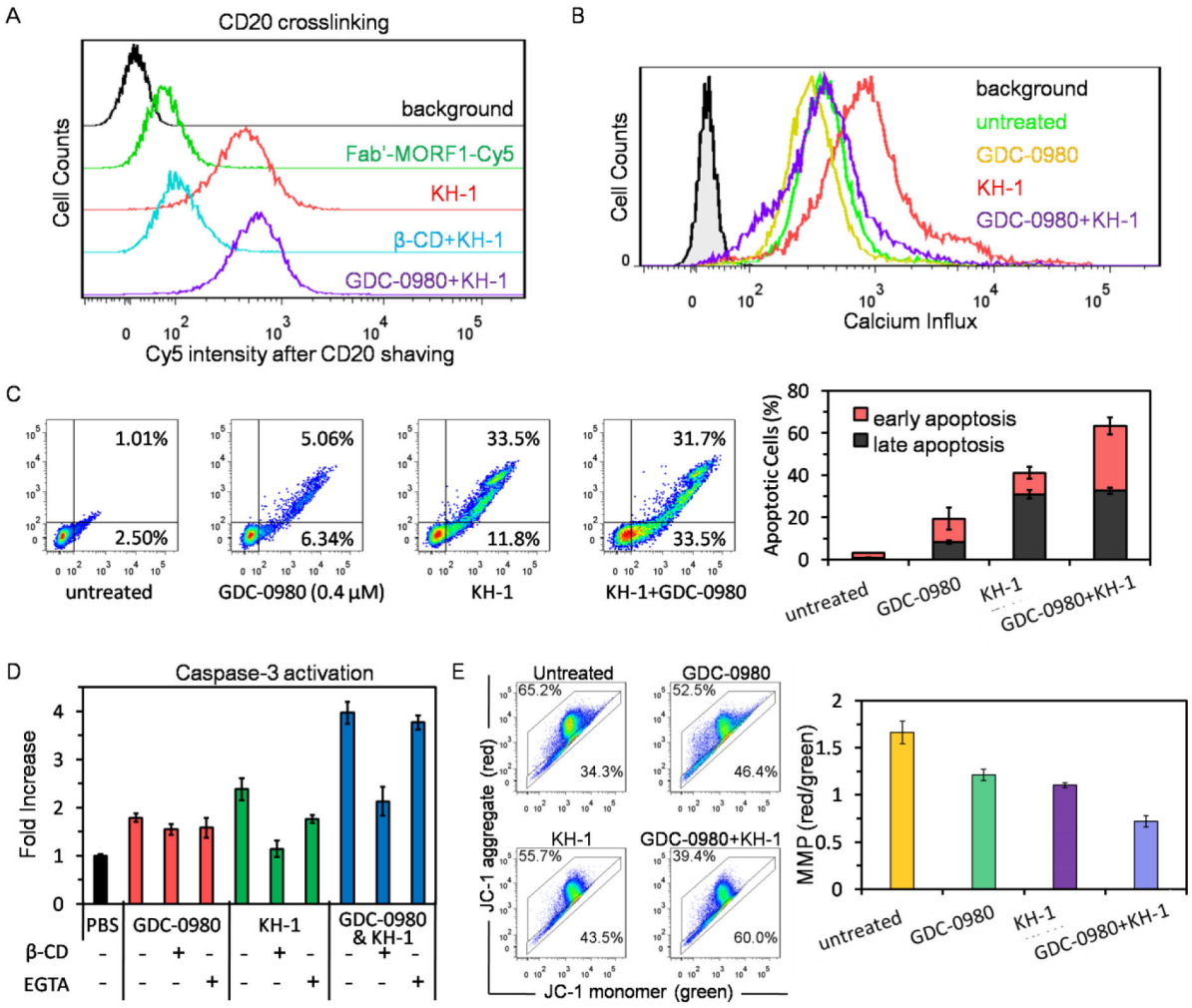

Figure 5.

(A) CD20 crosslinking, (B) calcium influx, (C) apoptosis induction, (D) caspase-3 activation, (E) mitochondrial depolarizationin Raji cells after treatment with GDC-0980 (0.4 μM, 24 h), KH-1 Fab'-MORF1 (1μM, 1h)/HSA-$(MORF2)_{13}$ (1μM MORF2, 24 h), or their combination.

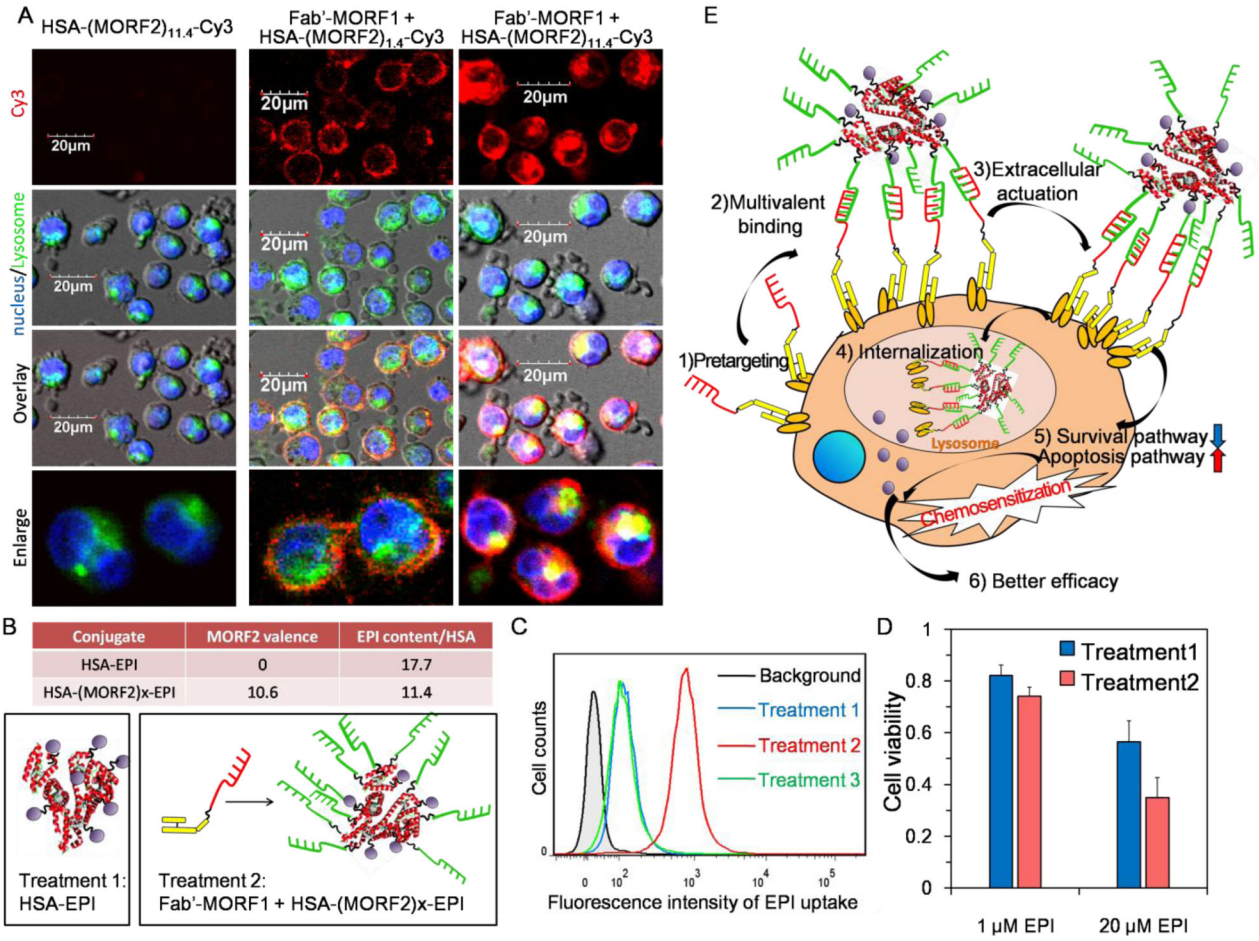

Figure 6.

(A) Raji cells were treated with (i) HSA-$(MORF2)_{11.4}$-Cy3 (1μM MORF2, 5 h), (ii) Fab'-MORF1(1μM MORF1, 1 h)→HSA-$(MORF2)_{1.4}$-Cy3 (1μM MORF2, 5 h), and (iii) Fab'-MORF1 (1μM MORF1, 1 h)→HSA-$(MORF2)_{11.4}$-Cy3 (1μM MORF2, 5 h), and then lysosomes and nuclei were stained, prior to confocal imaging. Red: Cy3; Green: lysosomes; Blue: nuclei. (B) Characterizations of epirubicin (EPI) conjugated HSA system: HSA-EPI and HSA-$(MORF2)_x$-EPI. (C) Cell uptake of EPI after Raji cells received treatment 1: HSA-EPI (20 μM EPI, 5 h); treatment 2: Fab'-MORF1 (1μM MORF1, 1 h)→HSA-$(MORF2)_x$-EPI (20 μM EPI, 5 h); or treatment 3: Fab'-MORF1 (1μM MORF1, 1 h)→HSA-EPI (20 μMEPI, 5 h). (D) Viabilities of Raji cells after treatment 1= HSA-EPI or treatment 2: Fab'-MORF1 (1μM MORF1, 1 h)→HSA-$(MORF2)_x$-EPI at 1 μM or 20 μM EPI equivalence for 48 h. (E) Schematic illustration of Fab'-MORF1/HSA-$(MORF2)_x$-drug system.